Phosphate removal from water by naturally occurring shale, sandstone and laterite: the role of iron oxides and soluble species

Dan Eude Kpannieu[1,2], Martine Mallet[1], Lacina Coulibaly[2], Mustapha Abdelmoula[1], Christian Ruby*[1]

[1]*Laboratoire de Chimie Physique et Microbiologie pour les Matériaux et l'Environnement - LCPME UMR 7564 CNRS-Université de Lorraine, 405 rue de Vandoeuvre, 54600 Villers-lès-Nancy (France)*

[2]*Laboratoire d'Environnement et Biologie Aquatique, Université Nangui Abrogoua, 02 BP 801, Abidjan 02 (Côte d'Ivoire)*

*Corresponding author. Tel.: ++33 3 72 74 74 09; fax: +33 3 83 27 54 44

E-mail address: Christian.ruby@univ-lorraine.fr (C. Ruby)

Abstract

The efficiency of phosphate removal from aqueous media by geomaterials from Ivory Coast, was evaluated, in batch and column experiments. Batch experiments showed that phosphate uptake strongly depended on pH. In addition, dissolution processes were less pronounced for laterite and sandstone compared to shale. A correlation between aqueous species concentrations due to shale dissolution and phosphate uptake was observed. The kinetics were well described using the pseudo-second order model. Isotherms displayed a saturation level on shale while phosphate uptake continuously increased for laterite and sandstone. The removal efficiency decreased in the following ranking order laterite > sandstone > shale. Laterite was also the most efficient adsorbent in column experiments. The high phosphate removal efficiency of laterite was attributed to the presence of superparamagnetic low grain sizes of goethite. Therefore

laterite is a particularly promising material for further investigation in wastewater treatment technology such as constructed wetlands.

Keywords: phosphate; adsorption; iron, geomaterials; Ivory Coast

1. Introduction

Phosphorous is an essential nutrient for the growth of aquatic plants and algae but its excessive supply in water bodies causes eutrophication resulting in increased growth of algae, the depletion of oxygen and the disruption in the balance of organisms. Excessive phosphate inputs to waters originates from anthropogenic activities such as wastewaters discharges and agricultural run-off. In wastewater treatment technology, chemical and biological removal techniques are the most effective and well-established methods but their high cost and complexity of implementation prevent their application both in rural areas and in developing countries. Recently, attention has been focused on developing alternative methods for phosphate removal from water. Among these methods, adsorption appears as an attractive option, owing to its low cost and easy application (Boyer et al., 2011; Hongbin and Ming, 2014). A large variety of materials with the availability to remove phosphate were thus described in the literature (Johansson-Westholm, 2006; Vohla et al., 2011, Wendling et al, 2013). High sorption capacity, low cost, availability in large quantity and environmentally-friendly nature are among the most important parameters in the choice of the sorbent. The present paper aimed to develop a material satisfying all these criteria with the final objective of applying this optimized material in the treatment of wastewater released into the Ebrié lagoon in Ivory Coast. In fact, the eutrophication of the Ebrié lagoon is dramatic in large areas, making the lagoon actually unsafe for habitation sites, for the practice of lucrative activities such as bathing and fishing (Briton et al., 2007; Koffi et al., 2009; Tuo et al., 2012; Yao et al., 2009). In this context,

shale, sandstone and laterite are natural geological materials easily available in large quantities in Ivory Coast. These low cost and environmentally friendly materials contain iron, calcium and aluminum and are thus expected to be promising phosphate adsorbents.

The main objective of the present study was to assess and compare the removal efficiencies of these three materials. Batch adsorption experiments were carried out as a function of adsorbent dosage, pH and contact time. The adsorption kinetics and Langmuir and Freundlich isotherms were also studied. Then, the performance of the three materials for phosphate removal were evaluated in flow through column experiments. The originality of the present work lied in the understanding of the relation existing between the physicochemical properties of the adsorbents and their ability to remove phosphate from water. A particular attention was devoted to quantify the dissolution properties of the minerals (release of Fe^{II}, Al^{III},, Mg^{II}, Ca^{II} in solution) in order to estimate the respective roles of dissolution precipitation and adsorption processes in the phosphate removal from water. This study is a necessary preliminary work before using the best determined adsorbents in a constructed wetland system.

2. Materials and methods

2.1. Chemicals

All chemicals used were analytical grade. All experiments were conducted in polypropylene vessels that were soaked in 36% hydrochloric acid (HCl) before use and rinsed with deionized water (Milli-Q, 18.2 MΩ cm^{-1}) and ethanol. Deionised water was used for preparing all solutions.

2.2. Adsorbent.

Shale, sandstone and laterite were collected in three regions of Ivory Coast, *i.e.* shale from the Center region (Toumodi-Lomo North), sandstone from the south region (Abidjan-Akouedo) and laterite from the Eastern region (Abengourou-Sankadjo). Samples were prepared using the

same following procedure. Large blocks extracted from the soil were first coarsely screened, washed with deionised water to remove the surface-adhered particles and dried in an oven at 50°C for 24 hours. The samples were then crushed again and sieved (AFNOR sieves) to obtain a granular size < 400 µm. Powder samples were finally washed again and dried at 70°C for 24 hours before their use. The chemical composition of the three substrates (Table 1) revealed that all three materials were primarily a mixture of oxides, the major one being SiO_2, Al_2O_3 and Fe_2O_3. The relative amount of these oxides differed from one material to the other. Sandstone was iron-rich while shale and laterite were Al-rich materials. All three subtrates contained large amount of Si. The specific surface area of the three powders materials (< 400 µm) was determined by multipoint N_2-BET analysis using a Belsorp max surface area analyser (Bel, Japan). The specific surface area of shale, sandstone and laterite were 6.3, 28.5 and 37.6 $m^2\ g^{-1}$ respectively.

2.3. Adsorption studies.

Phosphate adsorption onto the three substrates was studied in both batch and column experiments at room temperature. A stock phosphate solution (250 mg L^{-1}) of phosphate was prepared by using sodium dihydrogen phosphate ($H_2NaO_4P.2H_2O$) and diluted in subsequent experiments.

2.3.1. Batch experiments.

The effect of sorbent dose was examined in a series of experiments that used the same initial phosphate concentration (25 mg $PO_4\ L^{-1}$) while using different adsorbent doses between 0 and 160 g L^{-1}. 50 mL flasks were used. The pH of the suspension was maintained at a defined value of 6.5-7.0 by manually adding 0.5 M HCl or 0.5 M NaOH at regular intervals. Flasks were capped and stirred magnetically at 300 rpm for 24 hours to ensure approximate equilibrium. At the end of this adsorption period 10 mL were withdrawn from the reaction flasks and filtered through 0.22 µm polypropylene syringe filters for phosphate and aqueous metal species (Ca,

Mg, Al and Fe) analyses by ICP-AES. All experiments were carried out in duplicate to check the reproducibility of the experiments. The pH effect on phosphate adsorption was examined with a similar procedure using a 25 mg L^{-1} initial phosphate concentration and 80 g L^{-1} (shale) and 80 and 8 g L^{-1} (sandstone and laterite) adsorbent dosages while maintaining pH at different values in the range 2-12. Phosphate sorption kinetics were examined in 1 L Erlenmeyer flasks, using an initial phosphate concentration of 25 mg L^{-1}, various adsorbent doses, and for ~ 60 h. During this reaction period, samples were withdrawn from the flasks at regular intervals for phosphate and aqueous metal species determination. The pH of the suspension was maintained at a defined value (6.5-7.0). Sorption isotherms experiments were carried out at pH = 6.5-7.0 in 50 mL Erlenmeyer flasks with varying initial concentrations of phosphate ions (5-250 mg L^{-1}) and a constant adsorbent dosage of 80 g L^{-1} (shale) and 8 g L^{-1} (sandstone and laterite). The removal efficiency R (%) of phosphate onto adsorbents and phosphate uptake q_t (mg g^{-1}) at time *t* were calculated from Eqs 1-2:

$$R = \frac{(C_i - C_t)}{C_i} \quad \textbf{(1)}$$

$$q_t = \frac{(C_i - C_t) \times V}{m} \quad \textbf{(2)}$$

where C_i and C_t are the initial and at time *t* phosphate concentration (mg L^{-1}) respectively; V is the volume of the solution (L) and m is the mass of material (g). Note that phosphate uptake at near equilibrium conditions (q_e, mg g^{-1}) is obtained at the equilibrium phosphate concentration $C_t = C_e$.

2.3.2. Column experiments.

Plexiglas columns of 500 mm length and 37 mm internal diameter corresponding to a volume V_{tot} of 473 mL were used. The columns were packed with dried shale, sandstone or laterite (grain size of 1-2 mm) corresponding to a total mass of 593, 661 and 679 g, respectively. The porosity of all substrates was very close from 50 %; indeed the porous volume V_P for the three

materials was very similar, *i.e.* V_P = 236, 246 and 241 mL for shale, sandstone and laterite, respectively. An upwards water flow direction was used with the help of a peristaltic pump (Watson Marlow) ensuring by this way water-saturated conditions. All the columns were first pre-equilibrated with demineralized water during 24 hours before performing the phosphate removal experiments. The pH of the phosphate solution ($[PO_4]$ = 25 mg L^{-1}) introduced into the column was close to 5 and the pH measured in the outflow was relatively constant independently of the nature of the materials used in the columns with a mean pH value of 6.1, 6.0 and 6.4 for shale, sandstone and laterite, respectively. For both sandstone and laterite columns, a continuous flow of 1 mL min^{-1} with a corresponding Hydraulic Retention Time (HRT) of ~ 4 hours was used. The total duration of the experiments was ~ 2.5 months. In order to mimic situations that can be encountered in constructed wetlands where water supply is often provided discontinuously, a water flow circulating discontinuously was used for the shale column as described in our previous work (Kpannieu et al., 2018). The water flow was 0.23 mL min^{-1} during a first period of 104 hours with a corresponding HRT ~ 17 hours followed by a shutdown of the water pump corresponding to a HRT of ~ 64 hours. The sequence (104 hours, 64 hours) was repeated 9 times for a total duration of the experiments of ~ 2 months. At appropriate time intervals, 10 mL of solution was sampled in the column outflow and filtered through 0.22 µm polypropylene syringe filters before phosphate and metal species were analyzed with ICP-AES.

2.4. Characterization methods

The structural properties of shale, sandstone and laterite were investigated with X-Ray Diffraction (XRD) and Mössbauer spectrometry. XRD patterns were acquired with a PANalytical X'Pert Pro Multipurpose diffractometer using Co Kα radiation (λ = 1.78026 Å; 40 kV, 40 mA). Diffraction patterns were obtained over a range of 10-85° 2θ range with a step size

of 0.036° and nominal time per step of 3 s. Transmission Mössbauer spectrometry was performed with a 50 mCi source of ^{57}Co in rhodium to identify and quantify iron phases. The Mössbauer spectra were calibrated relatively to the reference spectrum of a 25 µm thick pure iron foil recorded at room temperature. A cryostat equipped with a closed cycle helium station allows variable temperature measurement between 8 and 300 K. The spectra were fitted using Lorentzian shape lines and, in some cases, Voigt profile analyses, a convolution of a Gaussian distribution with a Lorentzian shape line, was used. Residual phosphate (PO_4-P) and metal species (Ca, Mg, Al and Fe) concentrations in solution were determined by Inductively Coupled Plasma-Atomic Emission Spectrometry (ICP-AES) using an Ultima spectrometer (HORIBA Jobin Yvon).

3. Results and discussion

3.1. Physicochemical properties of the adsorbents.

3.1.1. X-Ray Diffraction (XRD).

All three diffraction patterns (Fig.1) displayed strong reflection of quartz (SiO_2). Additional reflection lines of silicates minerals such as muscovite ($KAl_2(Si, Al)_4O_{10}(OH)_2$, albite (Na, Ca) $(Si, Al)_4O_8$) and clinochlore $(Mg, Fe)_5(Si_3Al)O_{10}(OH)_8$ were observed for shale while iron oxides such as goethite (α-FeOOH) and hematite (Fe_2O_3) were observed for sandstone and laterite. Such mineral phases agreed relatively well with chemical composition reported in Table 1 except the absence of iron bearing minerals in shale. Because iron is well known to play a key role in phosphate adsorption (Altundoğan and Tümen, 2001; Mallet et al., 2013) a closer examination of iron phase minerals contained in the three substrates was carried out using Mössbauer spectrometry.

3.1.2. Mössbauer spectrometry.

The Mössbauer spectra of sandstone and laterite recorded at room temperature (Fig. 2) exhibited both two magnetic sextets attributed to hematite α-Fe_2O_3 and goethite α-FeOOH and a ferric paramagnetic doublet D_1 (Table 2), in agreement with XRD analyses. Mössbauer analysis at lower temperature was needed to distinguish whether the paramagnetic doublet D_1 recorded at room temperature corresponded to iron oxides or to Fe^{III} species embedded into the structure of clays. The Mössbauer spectra of sandstone and laterite recorded at 9 K clearly showed that the doublet observed at 300 K has been transformed into a magnetic sextet attributed to α-FeOOH (Fig. 3) (Kone et al., 2009). The corresponding Mössbauer hyperfine parameters (Table 3) revealed that only a very low intensity (RA of ~ 3 %) paramagnetic doublet remained on the 9 K Mössbauer spectrum of laterite and could be attributed to structural Fe^{III} species into clays. Therefore, for both sandstone and laterite, Fe^{III} species were essentially included into ferric oxides (α-Fe_2O_3 and α-FeOOH) and the ferric doublet recorded at room temperature (Fig. 2) was attributed to superparamagnetic goethite (Janot et al., 1973). This meant that the size of some of the goethite particles in sandstone and laterite was quite small. This must be particularly true for laterite since the ferric doublet recorded at room temperature was relatively intense (RA of ~ 55 %) and narrow and did not exhibit any relaxation effect (Table 2). This last result may be correlated to the BET analysis showing that laterite had the highest surface specific area. The status of iron in shale was very different and the Mössbauer spectrum recorded at 12 K (Fig. 3) exhibited a ferric (D_1) and a ferrous (D_2) paramagnetic doublet. The total relative area of both doublets are relatively high representing ~ 2/3 of the total spectra. This meant that for the shale most of the iron species were embedded into the clay minerals on the contrary to sandstone and laterite where iron was present into iron oxides. However, the shale did also contain some iron in goethite as shown by the magnetic sextet of α-FeOOH observed at 12 K (Fig. 3).

3.2. Phosphate sorption in batch experiments

3.2.1. Effect of adsorbent dosage.

All three substrates displayed not surprisingly an increase in the removal efficiency with increasing adsorbent dosage (Fig. 4). A high removal efficiency of 100% was achieved with laterite and sandstone at 20 and 40 g L^{-1} respectively while removal efficiency remained less than 100 % in the whole sorbent dose studied for shale (Fig. 4a). In addition, the phosphate uptake strongly decreased as the dosage increased and reached a saturation level at high sorbent doses. Such results reflected that adsorbed phosphate species were distributed among more available sorption sites at high sorbent doses, thus decreasing the sorption capacity (Ádám et al., 2007; Babatunde et al., 2009).

3.2.2. Effect of pH on phosphate adsorption.

The pH is an important factor that strongly influences the phosphate adsorption mechanisms at the solid-solution interfaces.. Small amounts of phosphate are determined at pH values lower than 8 and 10 for sandstone and laterite respectively which indicated a phosphate removal efficiency close to 100 % (Fig. 5). Beyond these two pH values, phosphate concentration strongly increased. A different behaviour was observed for shale. In fact, an increase in phosphate concentration was observed in the pH range of 2-11 followed by a strong decrease beyond pH 11. The insert in Figure 5 displays the phosphate concentration determined in solution for a 8 g L^{-1} laterite and sandstone dosage. The phosphate concentration increased onto the whole pH range studied. It can thus be concluded that increasing the pH resulted in a decrease of phosphate removal efficiency (at phosphate removal efficiencies lower than 100 %) except for shale for which a stronger removal efficiency was observed at pH 12. With the exception of this high pH value, the phosphate removal efficiency of shale was much smaller than those for sandstone and laterite.

3.2.3. Ions concentration as a function of pH.

To further investigate the phosphate removal mechanism, aqueous ions release was studied as a function of pH (Fig. 6). Strong release of Ca, Mg and Al, and to a lesser extent, Fe was observed for shale in the low pH range and in comparison to sandstone and laterite. Dissolution processes are thus much more pronounced for shale. Aqueous ions concentrations were compared both in blank experiments and after adsorbents reaction with a 25 mg L^{-1} phosphate solution (Fig. 7). Interestingly sandstone and laterite clearly exhibited a different behaviour from shale. In fact, low amounts of Ca, Mg, Al and Fe were determined in solution after shale reaction with phosphate ions and whatever the pH was. Additionally, calcium and magnesium concentrations did not significantly differ in blank experiments and after phosphate reaction with sandstone and laterite even at a lower dosage of 8 g L^{-1} (data not shown).Some differences in ions concentrations were observed at low pH where the presence of phosphate ions induced an increase in Fe and Al dissolution processes in laterite and sandstone respectively. From Fig. 5 to 7, it clearly appeared that shale displayed a different sorption behaviour from those of sandstone and laterite. The lower influence of dissolution processes towards phosphate removal in case of sandstone and laterite combined to a much more efficient phosphate removal clearly suggested that phosphate sorption was dominated by dissolution/reprecipitation processes for shale and adsorption processes for sandstone and laterite.

3.2.4. Phosphate adsorption kinetics.

Adsorption kinetics were carried out at 80 g L^{-1} (shale) and 8 g L^{-1} (laterite and sandstone) sorbent doses (Fig. 8). Results obtained at additional sorbent doses for laterite and sandstone are displayed in supporting information (Figs S1 and S2). All curves displayed almost the same shape. The adsorption rate was rapid at the beginning of the experiments and then decreased until a pseudo plateau was reached. The first step may be due to phosphate adsorption at the

external surface of the sorbents while the second step probably reflected some slow sorption process due to phosphate diffusion into the pores of the sorbent (Sanyal and De Datta 1991; Yang et al., 2006). The strength of the adsorbent decreased in the following order: laterite > sandstone > shale. In particular, the observed maximal phosphate uptake determined from Figure 8 were 3.2, 2.8, and 0.23 mg g^{-1} for laterite, sandstone and shale respectively. The uptake capacities of laterite and sandstone were higher than those reported for other natural materials such as bauxite (0.6 mg g^{-1}) (Drizo et al., 1999), limestone (0.55 mg g^{-1}) (Drizo et al., 1999), zeolite (0.25 mg g^{-1}) (Drizo et al., 1999), dolomite (0.3 mg g^{-1}) (Pant et al., 2001) and apatite (0.41 mg g^{-1}) (Bellier et al. 2006). Additionally, all these literature data were obtained at higher initial phosphate concentrations (40-150 mg L^{-1}). The sorption capacity of shale was thus smaller than those of laterite and sandstone by more than a factor of 10. The common pseudo-first-order and pseudo-second order equations were used to modelize the experimental data using a linear fitting (eqs 3-4):

Pseudo-first-order equation: $$\log (q_e - q_t) = \log q_e - \frac{k_1 t}{2.303} \quad \textbf{(3)}$$

Pseudo-second-order equation: $$\frac{t}{q_t} = \frac{1}{k_2 q_e^2} + \frac{t}{q_e} \quad \textbf{(4)}$$

where q_e (mg g^{-1}) is the equilibrium adsorption amount, q_t (mg g^{-1}) is the amount of phosphate adsorbed at any time t and k_1 (min^{-1}) and k_2 (g mg^{-1} min^{-1}) are the pseudo first-order and pseudo second-order rate constants respectively.

The linear plots of phosphate sorption kinetics obtained and the corresponding kinetics parameters are given in Figure 9, Figure S3 and Table 4 respectively. The kinetic data could only be well described using the pseudo-second-order kinetic model. High correlation coefficients were in fact obtained and the equilibrium sorption amounts (q_{cal}) closely match the experimental data while the pseudo first-order-model did not fit the data. Similar kinetics results were reported in the literature for various phosphate adsorbents (Cai et al., 2012; Namasivayam

and Prathap 2005; Zhu et al., 2009). Such results indicated that the adsorption process of phosphate on these three materials may be based on chemisorption. As the sorbent dose increased and the other experimental conditions remained unchanged, the value of k_2 increased.

3.2.5. Phosphate adsorption isotherms.

Isotherms are commonly used to describe the sorption behaviour of a given adsorbent (Yang et al., 2014; Liu and Zhang, 2015).. The sorption behaviour of laterite and sandstone was clearly different from that of shale (Fig. 10a). As it is the case in most studies, the shale curve displayed a saturation point at which increasing the initial phosphate concentration did not cause a significant increase in the phosphate sorption capacity (Zhu et al., 2009). The presence of this saturation level allowed us fitting the data by using the common Langmuir and Freundlich models (Fig. 10b). The data were better fitted by using the Langmuir model. The Langmuir linear plot of shale is displayed in figure 10b and the obtained parameters for both Langmuir and Freundlich models are reported in Table 5. Isotherms obtained for laterite and sandstone did not display any saturation level which made the prediction of the sorption capacity unreliable. Such a behaviour has already been reported in the literature for phosphate sorption by substrates used in constructed wetlands and phosphate retention in filter materials such as shellsand and filtralite P® (Boeykens et al., 2017; Drizo et al., 1999). In any way, the maximum phosphate uptake varied between 0.48 for shale and 8.3 mg g^{-1} for laterite. Note that the shale dose was ten times higher than those of sandstone and laterite. The ranking order of the maximum sorption capacity was therefore again: laterite > sandstone > shale. Remind that the specific surface area of shale, sandstone and laterite were 6.3, 28.5 and 37.6 m^2 g^{-1} respectively. It thus appeared that the material with the lowest specific surface area had the lowest phosphate uptake capacity. One reason for this may be that phosphate sorption was decreased by limited available surface sorption sites in case of shale. Another reason explaining the lowest capacity of shale for phosphate removal was the status of iron. Indeed the shale contained the lowest

quantity of iron (Table 1) and the lowest proportion of Fe in iron oxides , *i.e.* 31 % in comparison with 97 % and 100 % observed for laterite and sandstone, respectively. Iron oxides particles, in particular those with low crystal size, are well known to be preferential adsorption sites for phosphate species. The superiority of laterite for phosphate removal in comparison with shale and sandstone may be correlated to the existence of goethite particles with very low crystal size as testified by the superparamagnetic behaviour observed for this mineral by room temperature Mössbauer spectroscopy. Interstingly, laterite and sandstone were found to exhibit, on a surface area normalized basis, similar sorption capacities close to 0.1 g m^{-2} (section 2.2.4.), thus suggesting that the difference in reactivity was due to a particle size effect in agreement with Mössbauer analysis.

3.3. Phosphate adsorption in hydrodynamic conditions: column tests.

The breaktrough curves of sandstone and laterite obained at a flow rate of 1 mL min^{-1} and a corresponding HRT of ~ 4 hours are presented in Figure 11. We noticed that the breakthrough curve of laterite presented unsual shape with 2 plateaus. The origin of this behaviour was outside of the scope of the present study. As expected from the batch experiments, the breakthrough observed for laterite occured later than the one observed for sandstone. Indeed, if a threshold of $[PO_4]$ = 1 mg L^{-1} was chosen, *i.e.* C / C_0 of 0.04 with C_0 = 25 mg L^{-1}, the breakthrough occured at V / V_P of ~ 147 and 132 for laterite and sandstone, respectively. These values were about 8 times higher than the breakthrough observed previously for shale, *i.e.* V / V_P of ~ 17, even though the mean HRT of ~ 35 hours used for shale was much higher than the one used for sandstone and laterite. Therefore the column experiments confirmed that the capacity of shale to remove phosphate was the lowest as already observed in the batch experiments. The removal capacity at the breakthrough q_{break} can be computed to be q_{break} = 0.17, 1.23 and 1.30 mg PO_4 g^{-1} for shale, sandstone and laterite respectively. Calcium, magnesium and phosphate ions concentrations are displayed as a function of time (Fig.12) The

initial calcium (4.9 and 9.2 mg L^{-1} for laterite and sandstone, respectively), magnesium (1.8 and 1 mg L^{-1}), aluminum (not detected) and iron (not detected) concentrations in the outflow were in good agreement with the equilibrium data recorded at a pH of 5 in batch experiments. The soluble calcium and magnesium concentrations in the outflow decreased continuously and reached a value lower than 0.5 mg L^{-1} at the breakthrough. Experiments carried out in hydrodynamic mode required a preliminary step in which the column was pre-equilibrated with ultra-pure water during 24 h before the phosphate solution flowed through the column. The aqueous species concentrations determined at t =0 thus reflected the equilibria solubility that occurred during this period (Fig.12). In this experimental situation, phosphate removal partially occurred through reaction with the soluble species released in solution during the column equilibration. In fact, a correlation between the decrease in Ca and Mg concentrations and the increase in phosphate concentration at the outflow of the column was evidenced. Iron concentration as a function of time remained below the detection limit (data not shown). Such a behaviour had already been reported in the literature for shellsand and filtralite P® filter materials (Ádám et al., 2007). According to this study, phosphate removal occurred through the accumulation of large amounts of Ca (45-260 mg L^{-1}) and Mg ions (5-65 mg L^{-1}) at the beginning of the column experiment. The removal capacity at the breakthrough measured for filtralite P® and shellsand can be calculated from the data provided in this previous work (Ádám et al., 2007) and was evaluated to be respectively ~ 0.6 and 0.9 mg PO_4 g^{-1} for a contact time of ~ 4 days. Therefore, the removal capacity of laterite and sandstone from Ivory Coast was at least of the same order of magnitude than the one reported for the shellsand from Hordaland Tørkeri in Norway, which was recognized as a very efficient granular natural material for phosphate removal in hydrodynamic conditions.

Conclusion

The removal of phosphate by three natural materials from Côte d'Ivoire was studied in homogeneous batch suspensions and in static/hydrodynamic conditions in column experiments. The investigations revealed that all three materials retained phosphate to various extents. Batch experiments showed that the most efficient phosphate adsorbent was laterite followed by sandstone and shale, the sorption efficiency of shale being strongly smaller than those of laterite and sandstone. The removal of phosphate by adsorption on iron oxides was certainly very limited in shale studied here since most of the iron species were situated in structural substitution into the bulk of the solid clay minerals. In contrast most of the iron in laterite and sandstone occurred as in iron oxides. Laterite was also the most efficient mineral for removing phosphate in flow through conditions with a phosphate removal capacity at the breakthrough higher than 1 mg-PO_4 g^{-1}. Therefore, laterite is a very promising mineral for performing extensive dephosphatisation treatments in Ivory Coast and neighbouring countries of Africa (Xue et al., 2009).

Acknowledgements

The authors thank G. Medjahdi (Centre of X-gamma Competence; UMR 7198 CNRS - Université de Lorraine, Nancy-France) for DRX analyses and C. Genois from the LCPME is gratefully acknowledged for ICP analyses.

References

Ádám, K., Krogstad, T., Vråle, L., Søvik, A. K., Jenssen, P.D., 2007. Phosphorus retention in the filter materials shellsand and filtralite P® -Batch and column experiment with synthetic P solution and secondary wastewater. Ecol. Engineer. 29, 200-208.

Altundoğan, H.S., Tümen, F., 2001. Removal of phosphates from aqueous solutions by using bauxite. I: Effect of pH on the adsorption of various phosphates. J. Chem. Technol. Biotechnol. 77, 77-85.

Babatunde, A.O., Zhao, Y.Q., Burke, A.M., Morris, M.A., Hanrahan, J.P., 2009. Characterization of aluminium-based water treatment residual for potential phosphorus removal in engineered wetlands. Environ Pollut. 157, 2830-2836.

Boeykens, S.P., M., Piol, N., Legal, L.S., Saralegui, A.B., Vazquez, C., 2017. Eutrophication decrease: Phosphate adsorption processes in presence of nitrates. J. Environ. Manage. 203, 888-895.

Boyer, T.H., Persaud, A., Banerjee, P., Palomino, P., 2011. Comparison of low-cost and engineered materials for phosphorus removal from organic-rich surface water. Water Res. 45, 4803-4814.

Briton Bi, G.H., Yao, B., Ado, G., 2007. Evaluation of the Abidjan lagoon pollution. J. Appl. Sci. Environ. Manage. 11 (2) 173-179.

Cai, P., Zheng, H., Wang, C., Ma, H., Hu, J., Pu, Y., Liang, P., 2012. Competitive adsorption characteristics of fluoride and phosphate on calcinated Mg-Al-CO3 layered double hydroxides. J.Hazard. Mat. 213-214, 100-108.

Drizo, A., Frost, C.A., Grace, J., Smith K.A., 1999. Physicochemical screening of phosphate-removing substrates for use in constructed wetland systems. Water Res. 33, 595-3602.

Hongbin, Y., Ming, K., 2014. Simultaneous removal of ammonium and phosphate from eutrophic waters using natural calcium-rich attapulgite-based versatile adsorbent. Desalination. 351, 128-137.

Janot, C., Gibert, H., Tobias, C., 1973. Caracterisation de kaolinites ferrifères par spectrométrie Mössbauer. Bull. Soc. Fr. Mineral. Cristallogr. 96, 281-291.

Johansson-Westholm, L., 2006. Review- Substrates for phosphorus removal-Potential benefits for on-site wastewater treatment? Water Res. 40(1), 23-36.

Koffi, S.O., Coffy, A.A., Villeneuve, J.P., Sess, D.E., N'Guessan, Y.T., 2009. Pollution of a tropical lagoon by the determination of organochlorine coumpounds. Tropicultura. 27(2), 77-82.

Kone,T., Hanna, K., Abdelmoula, M., Ruby, C., Carteret, C., 2009. Reductive transformation and mineralization of an azo dye by hydroxysulphate green rust preceding oxidation using H2O2 at neutral pH. Chemosphere. 75, 212-219.

Kpannieu, D.E., Ruby, C., Coulibaly, L., Abdelmoula, M., Mallet, M., 2018. Removal of phosphate by shale from Ivory Coast in homogeneous reactor and hydrodynamic conditions: influence of soluble species. Clays Clays Min. submitted.

Liu, X., Zhang, L., 2015. Removal of phosphate anions using the modified chitosan beads: Adsorption kinetic, isotherm and mechanism studies. Powder Technol. 277, 112-119.

Mallet, M., Barthélémy, K., Ruby, C., Renard, A., Naille, S., 2013. Investigation of phosphate adsorption onto ferrihydrite by X-ray Photoelectron Spectroscopy. J. Colloid Interf. Sci. 407, 95-101.

Namasivayam, C., Prathap, K., 2005. Recycling Fe(III)/Cr(III) hydroxide, an industrial solid waste for the removal of phosphate from water. J. Hazard. Mat., 2005, 123 (1-3), 127-134.

Pant, H.K., Reddy, K.R., Lemon, E., 2001. Phosphorus retention capacity of root bed media of subsurface flow constructed wetlands. Ecol. Eng. 17, 345-355.

Sanyal, S.K., De Datta, S.K., 1991. Chemistry of phosphorus transformation in soils, in: B.A. Stewart (Ed.), Adv. Soil Sci. 16, 1-94.

Stumm, W., 1997. Reactivity at the mineral-water interface: dissolution and inhibition. Colloids surf. A: Physicochem. Eng. Aspects. 120 (1-3), 143-166.

Tuo, A.D., Soro, M.B., Trokourey, A., Bokra, Y., 2012. Assessment of waters contamination by nutrients and heavy metals in the Ebrie Lagoon (Abidjan, Ivory Coast). Res. J. Environ. Toxicol. 6 (5), 198-209.

Vohla, C., Kõiv, M., Bavor, H.J., Chazarenc, F., Mander, Ü., 2011. Filter materials for phosphorus removal from wastewater in treatment wetlands-A review. Ecol. Eng. 37(1), 70-89.

Wendling, L.A., Douglas, G.B., Coleman, S., Yuan, Z., 2013. Nutrient and dissolved organic carbon removal from natural waters using industrial by-products. Sci. Total Environ. 442, 63-72.

Yang, Y., Tomlinson D., Kennedy S., Zhao Y.Q. 2006. Dewatered alum sludge: a potential adsorbent for phosphorus removal. Wat. Sci. Tech. 54 (5), 207-213.

Yang, M., Lina, J., Zhana, Y., Zhang, H., 2014. Adsorption of phosphate from water on lake sediments amended with zirconium-modified zeolites in batch mode. Ecol. Eng. 71, 223-233.

Yao, K.M., Metongo, B.S., Trokourey, A., Bokra, Y., 2009. La pollution des eaux de la zone urbaine d'une lagune tropicale par les matières oxydables (lagune Ebrié, Côte d'Ivoire), Int. J. Chem. Sci. 3 (4), 755-770.

Xue, Y., Hou, H., Zhu, S., 2009. Characteristics and mechanisms of phosphate adsorption onto basic oxygen furnace slag. J. Hazard. Mat. 162(2–3), 973-980.

Zhu, M. X., Ding, K.Y., Xu, S.H., Jiang, X., 2009. Adsorption of phosphate on hydroxyaluminum-and hydroxyiron-montmorillonite complexes. J. Hazard. Mat. 165, 645-651.

Figure Captions

Fig. 1 - XRD patterns of naturally occurring shale, sandstone and laterite from Ivory Coast. The following abbreviations are used: A: Albite; B: Birnessite; C: Clinochlore; G: goethite; H: Hematite; M: Muscovite and Q: quartz.

Fig.2 - Mössbauer spectra of naturally occurring sandstone (a) and laterite (b) from Ivory Coast at room temperature.

Fig.3 - Mössbauer spectra of naturally occurring shale, sandstone and laterite from Ivory Coast at 12 K (shale) and 9 K (sandstone and laterite).

Fig. 4 - Phosphate removal efficiency (a) and phosphate uptake (b) for shale, sandstone and laterite as a function of adsorbent dose ($[PO_4]_{initial}$ = 25 mg L^{-1}; pH ~ 7; time contact: 24 h)

Fig. 5 - Phosphate concentration as a function of pH after sandstone, laterite and shale reaction with a 25 mg L^{-1} initial phosphate solution ([sorbent] = 80 g L^{-1} and 8 g L^{-1} (insert); pH ~ 7; time contact: 24 h)

Fig. 6 - Ions concentrations in solution in blank experiments as a function of pH ([adsorbent] = 80 g L^{-1}; pH ~ 7; time contact: 24 h).

Fig. 7 - Ions concentrations in solution in blank experiments and after reaction with a 25 mg L^{-1} initial phosphate solution ([sorbent] = 80 g L^{-1}; pH ~ 7; time contact: 24 h).

Fig. 8 - Effect of contact time on phosphate uptake capacity by sandstone, laterite and shale ($[PO_4]_{initial}$ = 25 mg L^{-1}; pH ~ 7; contact time: 24 h).

Fig.9 - Kinetics modelling of phosphate sorption onto shale (80 g/L) and sandstone and laterite (8 g/L) using pseudo-second order model ($[PO_4]_{initial}$ = 25 mg L^{-1}; pH ~ 7; time contact: 24 h).

Fig 10 - Adsorption isotherms of phosphate for the three different sorbents (a) and Langmuir plot for phosphate sorption onto shale (b); (pH ~ 7; time contact: 24 h).

Fig. 11 - Breakthrough curves obtained for the sandstone and laterite column experiment in hydrodynamic conditions (flow of 1 mL min^{-1}, C_0 = 25 mg PO_4 L^{-1}).

Figure 12 - Ca^{2+}, Mg^{2+} and PO_4^{3-} concentrations as a function of time in sandstone and laterite column experiments in hydrodynamic conditions (ϕ 1-2mm).

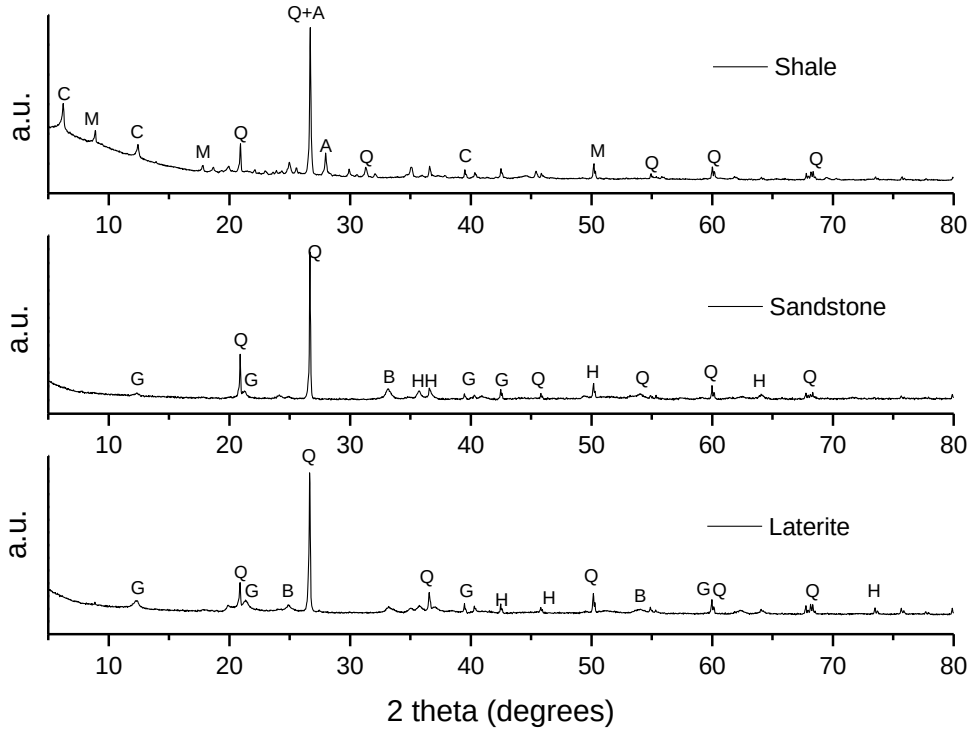


Fig. 1 - XRD patterns of naturally occurring shale, sandstone and laterite from Ivory Coast. The following abbreviations are used: A: Albite; B: Birnessite; C: Clinochlore; G: goethite; H: Hematite; M: Muscovite and Q: quartz.

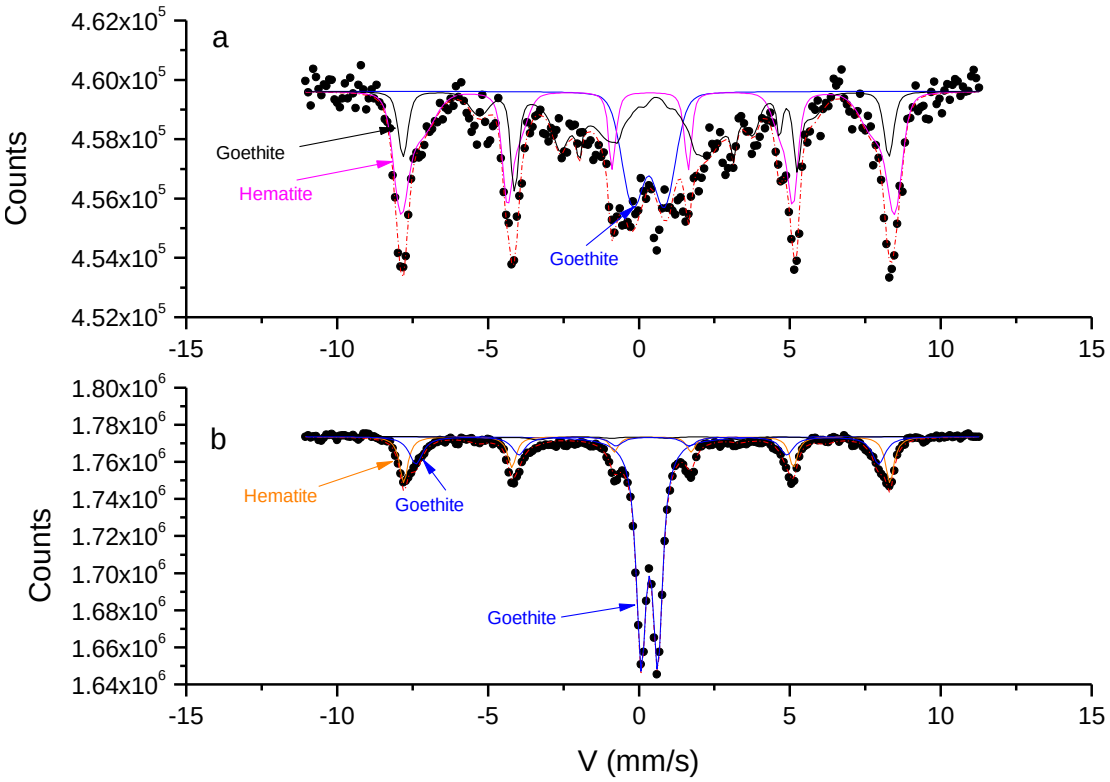


Fig.2 - Mössbauer spectra of naturally occurring sandstone (a) and laterite (b) from Ivory Coast at room temperature.

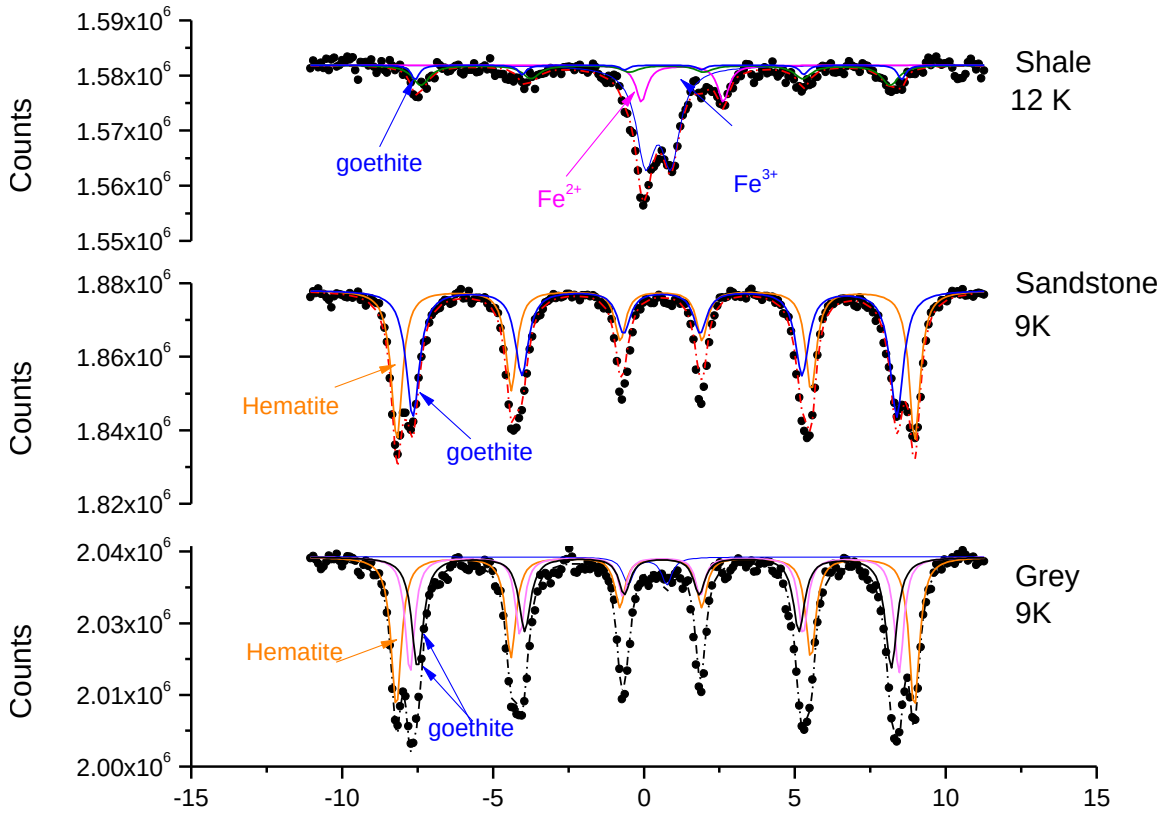


Fig.3 - Mössbauer spectra of naturally occurring shale, sandstone and laterite from Ivory Coast at 12 K (shale) and 9 K (sandstone and laterite).

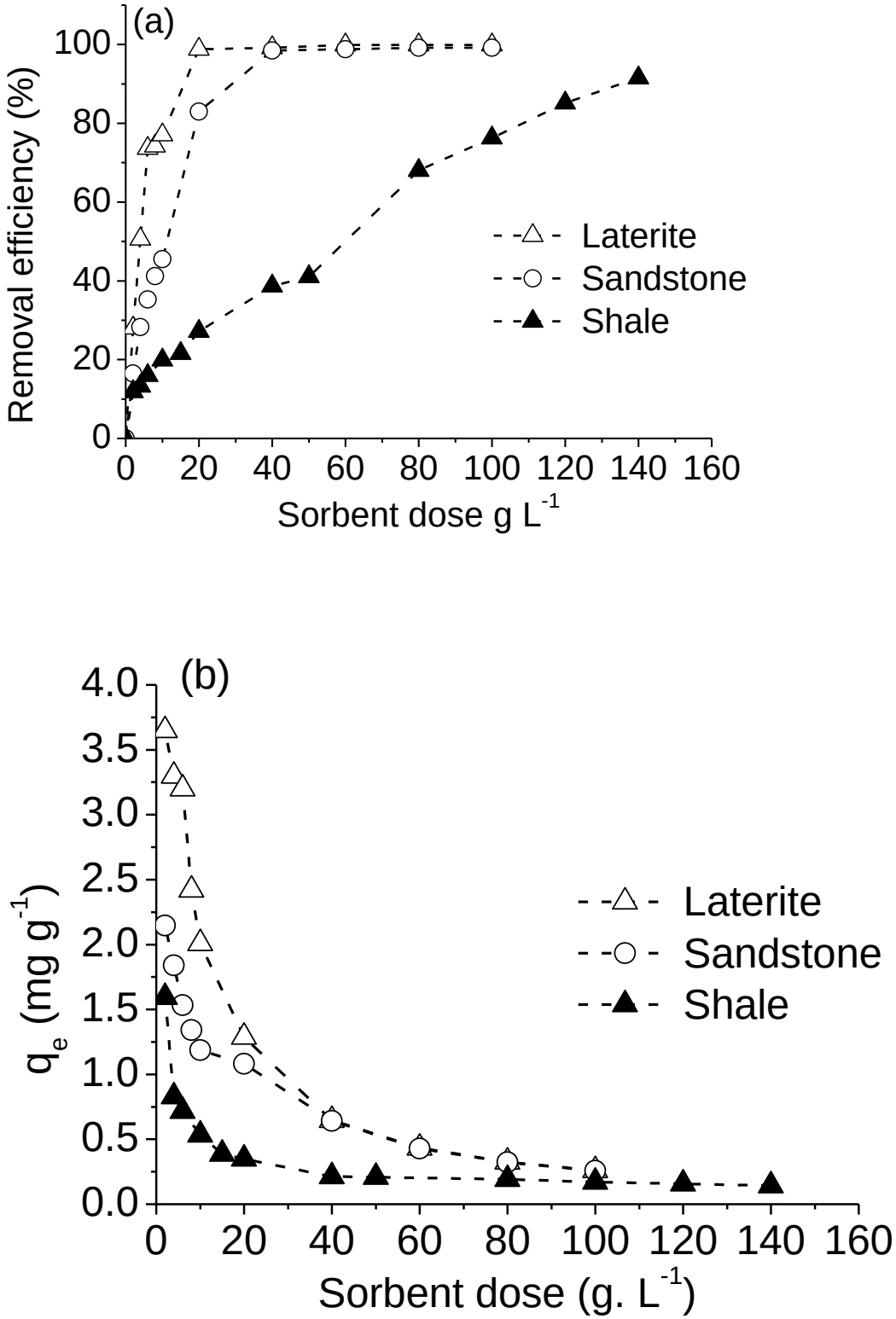


Fig. 4 - Phosphate removal efficiency (a) and phosphate uptake (b) for shale, sandstone and laterite as a function of adsorbent dose ($[PO_4]_{initial}$ = 25 mg L^{-1}; pH ~ 7; time contact: 24 h)

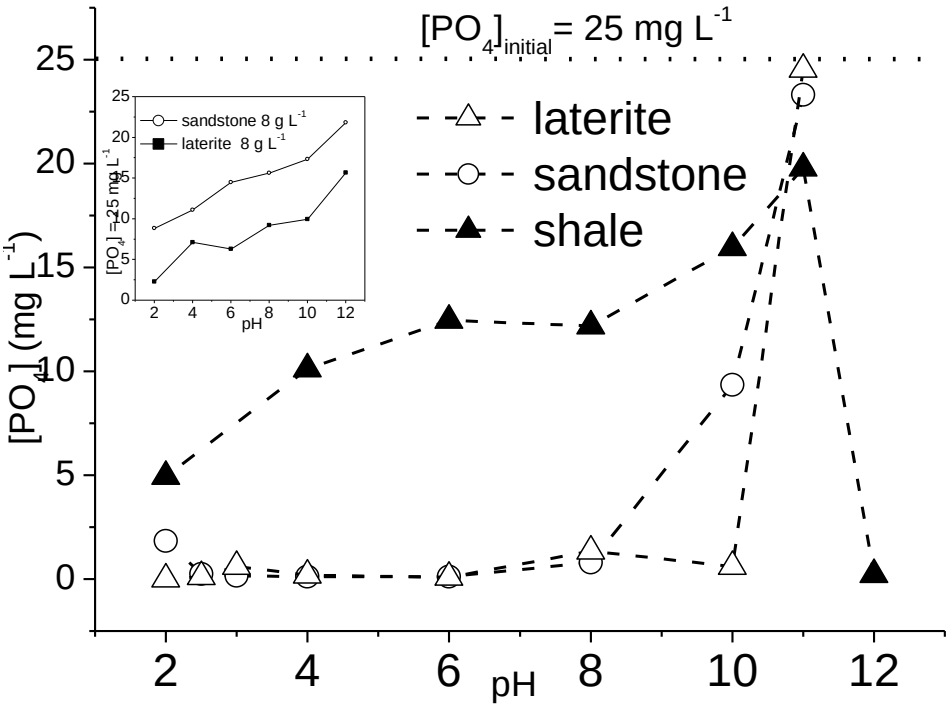


Fig. 5 - Phosphate concentration as a function of pH after sandstone, laterite and shale reaction with a 25 mg L^{-1} initial phosphate solution ([sorbent] = 80 g L^{-1} and 8 g L^{-1} (insert); pH ~ 7; time contact: 24 h)

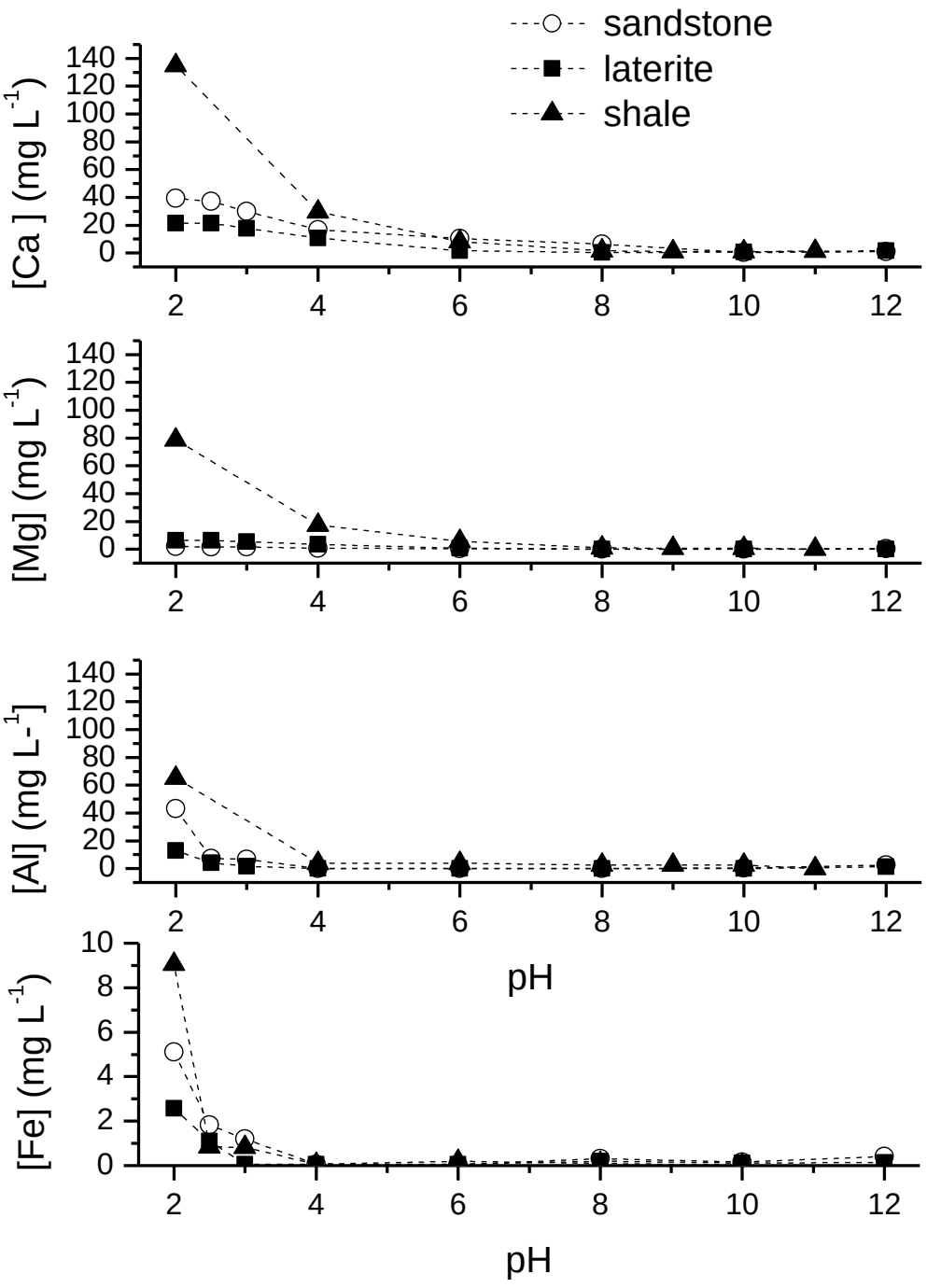
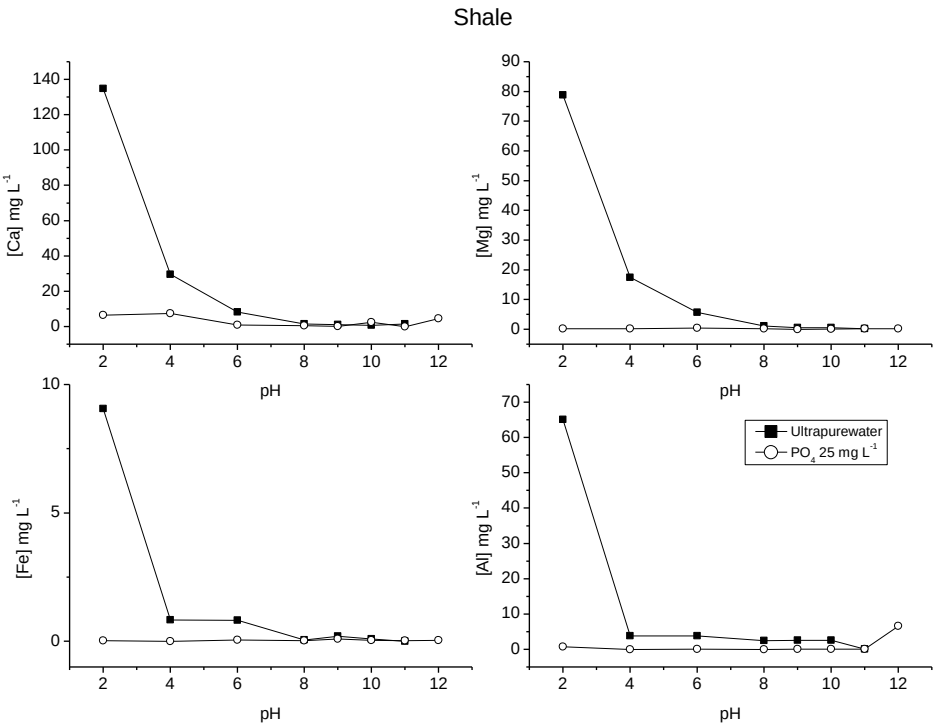
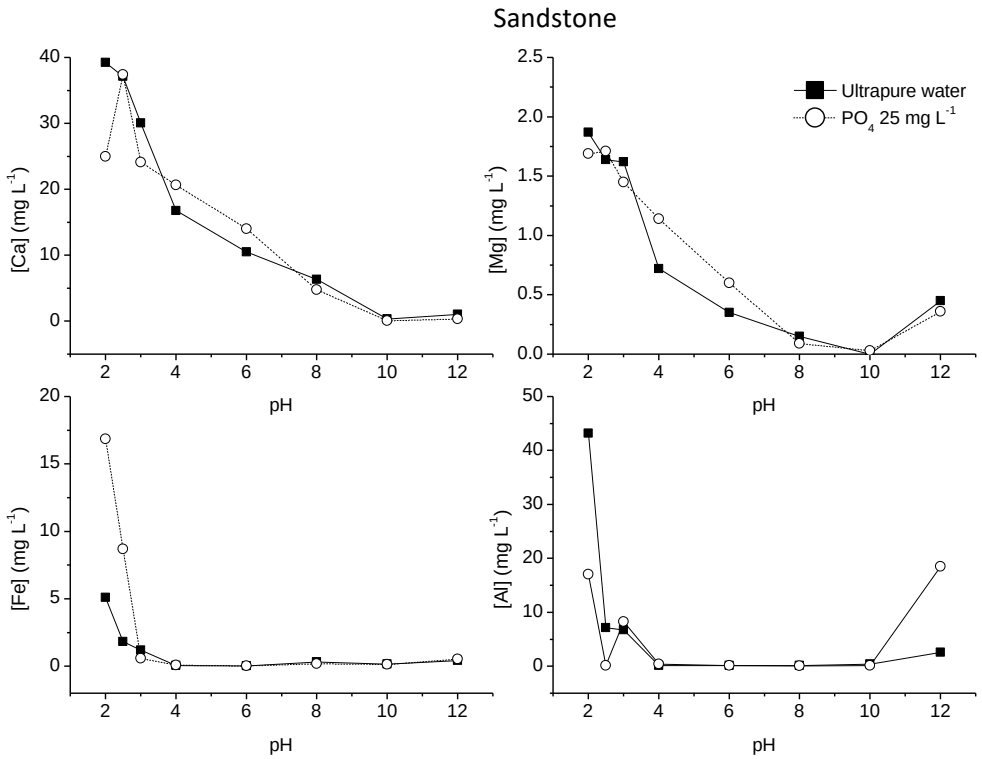


Fig. 6 - Ions concentrations in solution in blank experiments as a function of pH ([adsorbent] = 80 g L^{-1}; pH ~ 7; time contact: 24 h).


Shale
[Ca] mg L-1
[Mg] mg L-1
[Fe] mg L-1
[Al] mg L-1
pH
Ultrapurewater
PO4 25 mg L-1


Sandstone
[Ca] (mg L-1)
[Mg] (mg L-1)
[Fe] (mg L-1)
[Al] (mg L-1)
pH
Ultrapure water
PO4 25 mg L-1

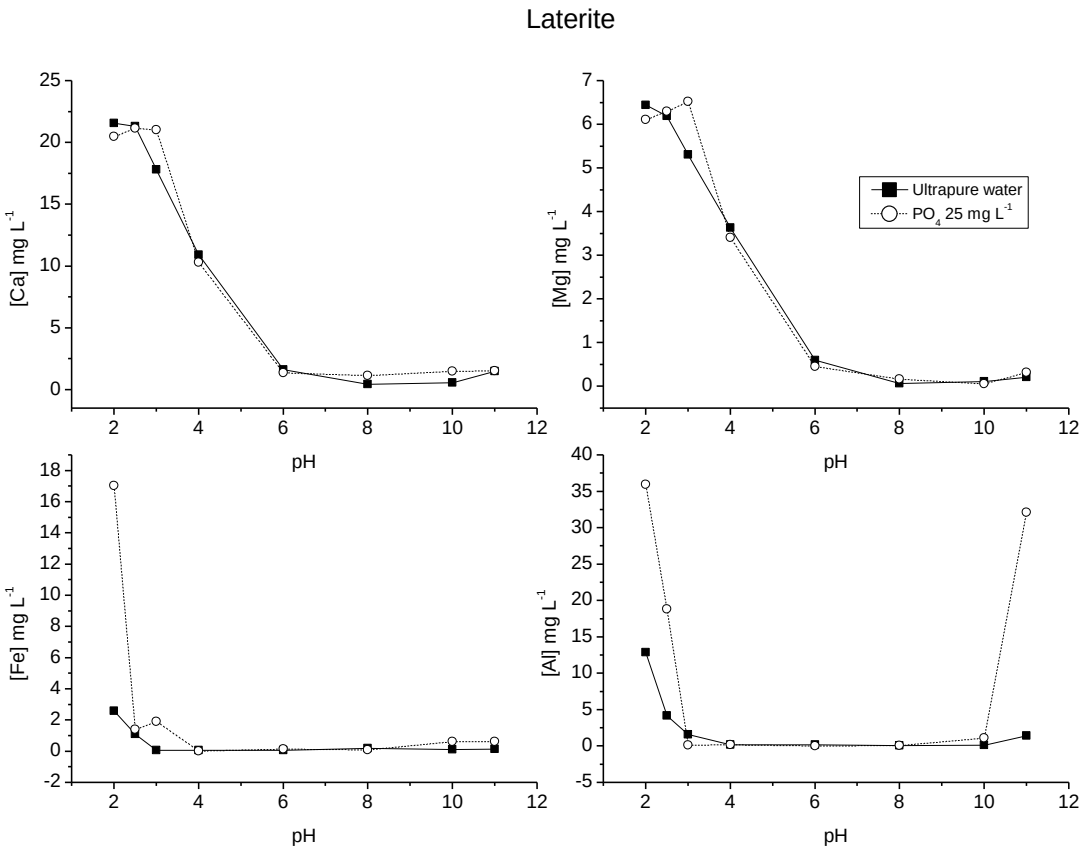


Fig. 7 - Ions concentrations in solution in blank experiments and after reaction with a 25 mg L^{-1} initial phosphate solution ([sorbent] = 80 g L^{-1}; pH ~ 7; time contact: 24 h).

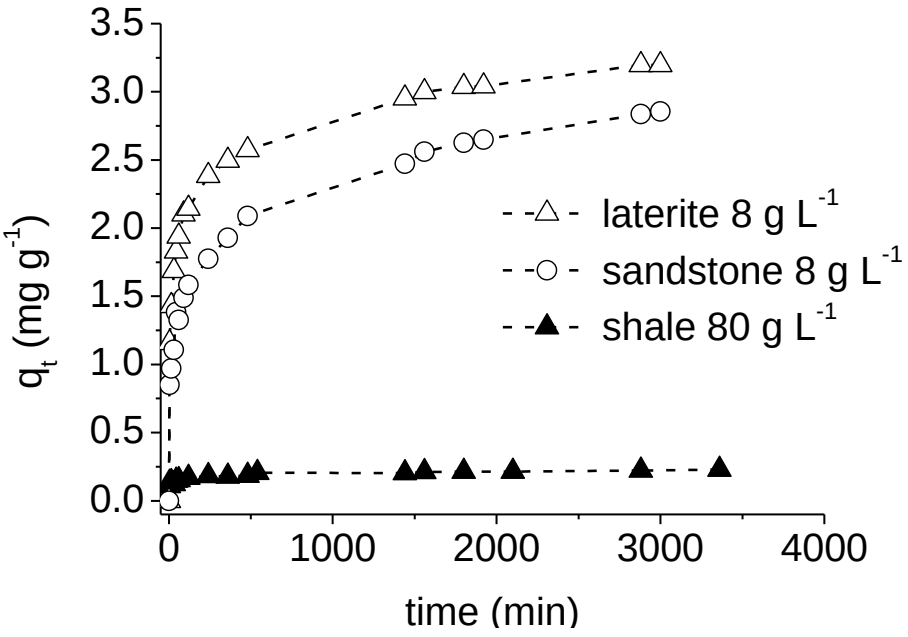
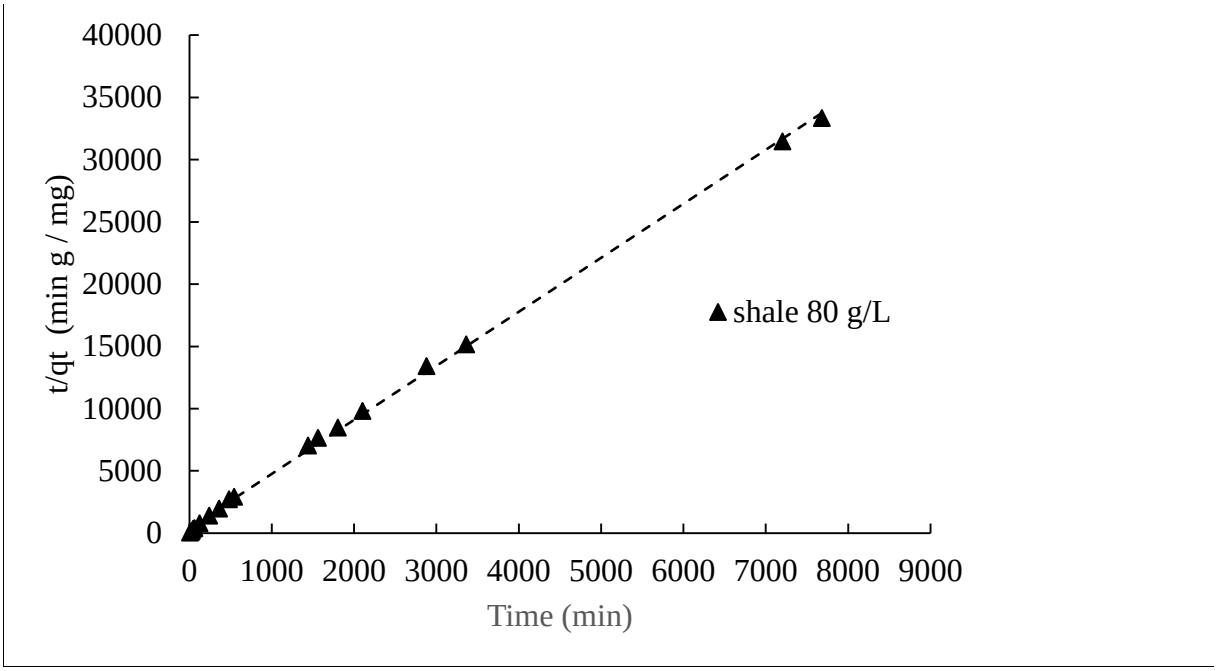


Fig. 8 - Effect of contact time on phosphate uptake capacity by sandstone, laterite and shale ($[PO_4]_{initial}$ = 25 mg L^{-1}; pH ~ 7; contact time: 24 h).



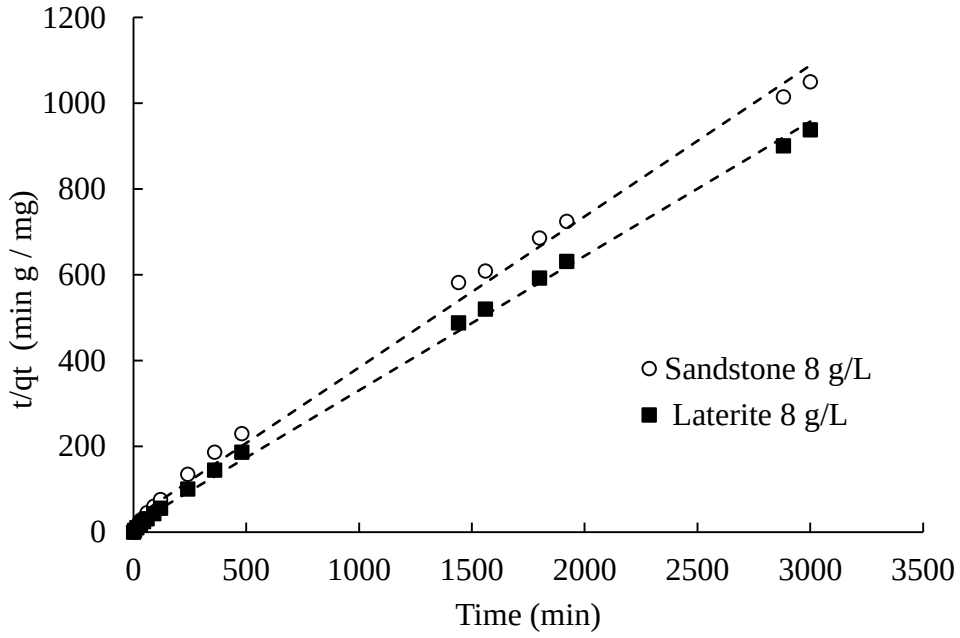


Fig.9 - Kinetics modelling of phosphate sorption onto shale (80 g/L) and sandstone and laterite (8 g/L) using pseudo-second order model ($[PO_4]_{initial}$ = 25 mg L^{-1}; pH ~ 7; time contact: 24 h).

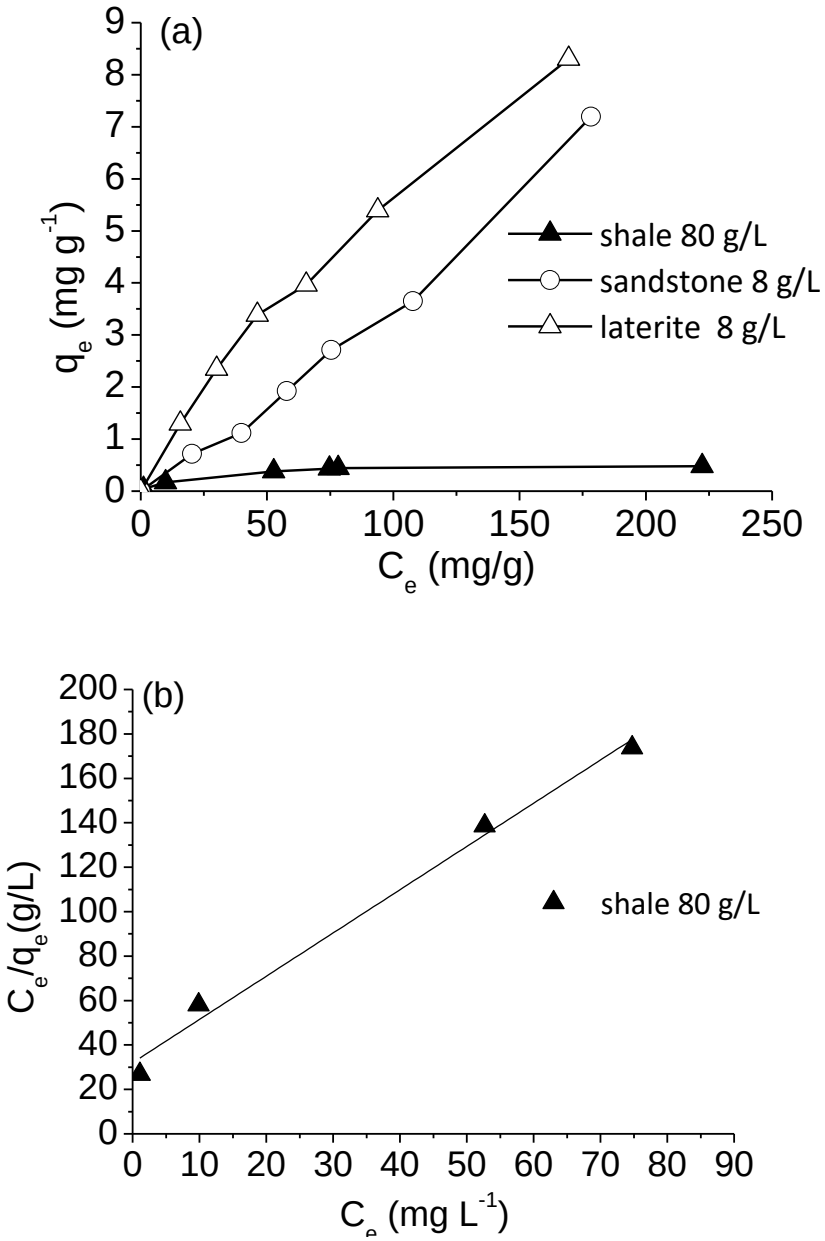


Fig 10 - Adsorption isotherms of phosphate for the three different sorbents (a) and Langmuir plot for phosphate sorption onto shale (b); (pH ~ 7; time contact: 24 h).

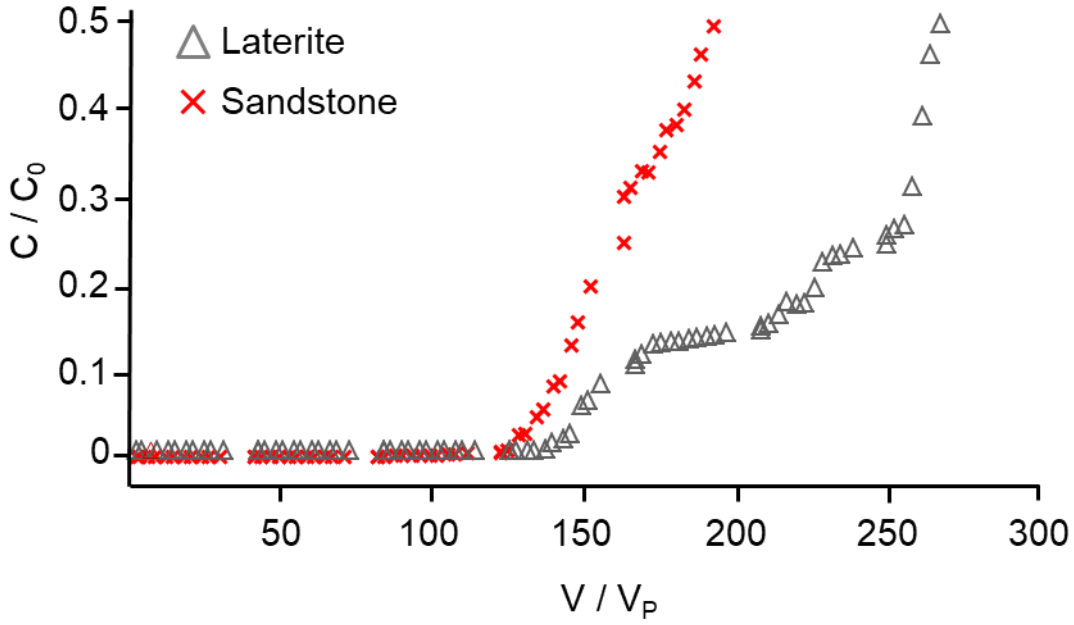


Fig. 11 - Breakthrough curves obtained for the sandstone and laterite column experiment in hydrodynamic conditions (flow of 1 mL min^{-1}, C_0 = 25 mg PO_4 L^{-1}).

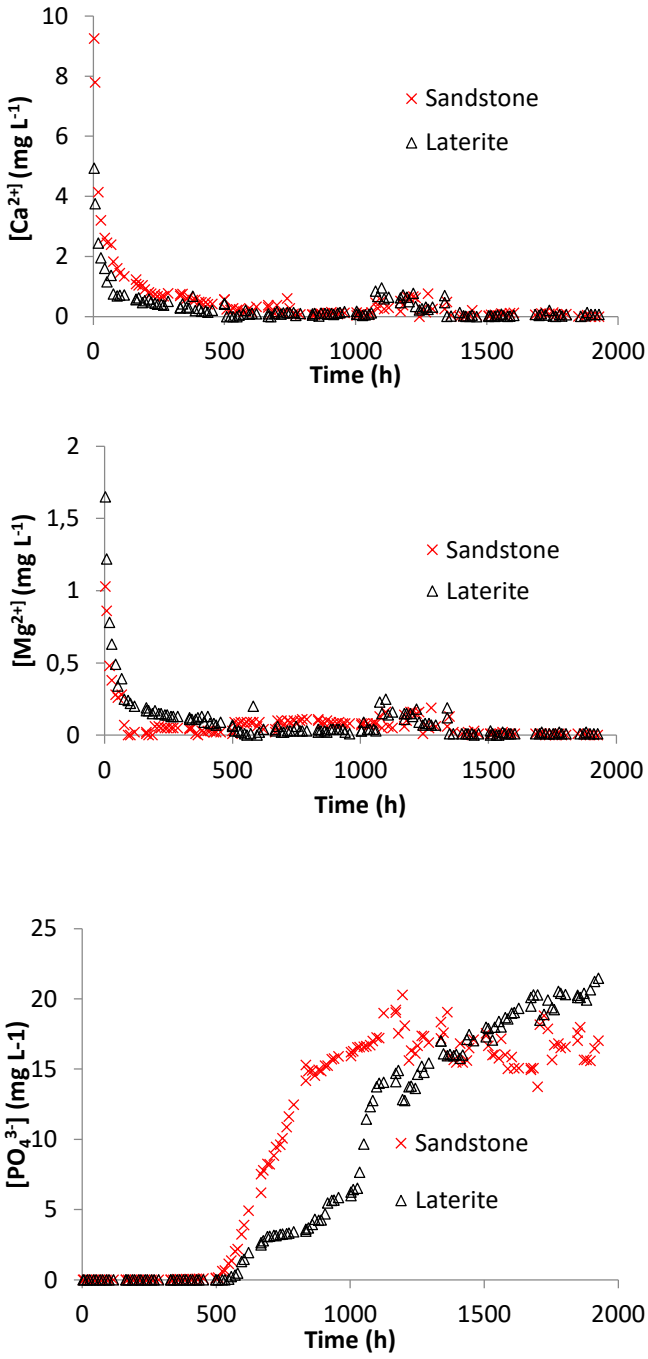


Fig. 12 - Ca^{2+}, Mg^{2+} and PO_4^{3-} concentrations as a function of time in sandstone and laterite column experiments in hydrodynamic conditions (ϕ 1-2mm).

Table captions

Table 1- Chemical composition (wt %) of naturally occurring shale, sandstone and laterite samples from Ivory Coast.

Table 2 - Mössbauer hyperfine parameters of the spectra of shale, sandstone and grey presented in Fig. 2. CS: center shift with respect to α-Fe at room temperature; Δ: quadrupole splitting or ε : quadrupole shift ; H hyperfine magnetic field and RA: Relative Area.

Table 3 - Mössbauer hyperfine parameters of the spectra of shale, sandstone and grey presented in Fig. 2. CS: center shift with respect to α -Fe at room temperature Δ: quadrupole splitting or Ɛ: quadrupole shift ; H hyperfine magnetic field and RA: Relative Area.

Table 4 - Kinetic models parameters for phosphate adsorption on laterite, sandstone and shale after reaction with an initial phosphate concentration of 25 mg L^{-1}.

Table 5 - Langmuir and Freundlich isotherm parameters for phosphate adsorption on shale (pH ~ 7; [shale] = 80 g/L; contact time: 24 h)

	SiO_2	Al_2O_3	Fe_2O_3	MnO	MgO	CaO	Na_2O	K_2O	TiO_2	P_2O_5	LoI*
Shale	56.8	17.5	10.2	0.6	2.1	0.4	0.9	2.4	1	0.1	8.7
Sandstone	29.3	6.3	54.4	<L.D.	<L.D.	0.1	<L.D.	0.1	0.3	1.0	8.7
Latérite	50.3	14.0	24.5	0.1	0.08	0.08	0.02	0.3	0.7	0.1	9.9

*****Loss on Ignition

Table 1 - Chemical composition (wt %) of naturally occurring shale, sandstone and laterite samples from Ivory Coast.

Name	Component	CS	Δ ou Ɛ	H	RA
		($mm.s^{-1}$)	($mm.s^{-1}$)	(kOe)	(%)
Sandstone	D1 (α-FeOOH)	0.32	1.07	-	19
	S1 (α-FeOOH)	0.41	-0.17	290	41
	S1 (Fe_2O_3)	0.37	-0.04	491	40
Laterite	D1 (α-FeOOH)	0.34	0.55	-	55
	S1 (α-FeOOH)	0.35	-0.26	340	6
	S1 (Fe_2O_3)	0.66	-0.1	500	20
	S1 (Fe_2O_3)	0.36	-0.09	476	19

Table 2 - Mössbauer hyperfine parameters of the spectra of shale, sandstone and grey presented in Fig. 2. CS: center shift with respect to α-Fe at room temperature; Δ: quadrupole splitting or ε : quadrupole shift ; H hyperfine magnetic field and RA: Relative Area.

Name	T (K)	Component	CS ($mm.s^{-1}$)	Δ ou Ɛ ($mm.s^{-1}$)	H (kOe)	RA (%)
Shale	12	D1 (Fe^{3+})	0.470	0.836	-	55
		D2 (Fe^{2+})	1.272	2.71	-	14
		S1 (α-FeOOH)	0.6	-0.2	480	23
		S2 (α -FeOOH)	0.56	-0.08	500	8
Sandstone	9	S1 (α -FeOOH)	0,48	-0.12	497	51
		S2 (Fe_2O_3)	0,48	-0.08	532	49
Laterite	9	S1 (α -FeOOH)	0.46	-0.12	502	28
		S2 (α -FeOOH)	0.46	-0.12	487	32
		S3 (Fe_2O_3)	0.46	-0.09	532	40
		D1 (Fe(III)))				3

Table 3 - Mössbauer hyperfine parameters of the spectra of shale, sandstone and grey presented in Fig. 2. CS: center shift with respect to α -Fe at room temperature; Δ: quadrupole splitting or Ɛ: quadrupole shift; H hyperfine magnetic field and RA: Relative Area.

			Pseudo-first-order kinetic model			Pseudo-second-order kinetic model		
Material	Dose ($g\ L^{-1}$)	q_{exp} ($mg\ g^{-1}$)	q_{calc} ($mg\ g^{-1}$)	k_1 (min^{-1})	R^2	q_{calc} ($mg\ g^{-1}$)	k_2 ($g\ mg^{-1}min^{-1}$)	R^2
Laterite	15	1.70	0.41	0.01	0.703	1.78	0.041	0.999
	8	3.2	1.31	0.01	0.926	3.2	0.006	0.998
Sandstone	80	0.99	0.29	0.01	0.927	0.99	0.51	1.000
	30	0.87	0.48	0.02	0.963	0.89	0.10	1.000
	8	2.8	1.80	0.01	0.800	2.84	0.01	0.990
Shale	80	0.21	0.07	0.01	0.955	0.23	0.04	0.999

Table 4 - Kinetic models parameters for phosphate adsorption on laterite, sandstone and shale after reaction with an initial phosphate concentration of 25 mg L^{-1}.

Model	Equation	Parameters	
Langmuir	$\frac{C_e}{q_e} = \frac{C_e}{q_m} + \frac{1}{K_L q_m}$	R^2	0.995
		q_m (mg/g)	0.514
		K_L(L/g)	0.061
Freundlich	$Ln(q_e) = Ln(K_f) + \frac{1}{nf} Ln(C_e)$	R^2	0.955
		n_f	2.02
		K_f (L/g)	0,046

Table 5 - Langmuir and Freundlich isotherm parameters for phosphate adsorption on shale (pH ~ 7; [shale] = 80 g/L; contact time: 24 h)